Spatial Aperture-Sampled Mode Multiplexer Extended to Higher Mode Count Fibers

Miri Blau and Dan M. Marom, *Senior Member, IEEE*

***Abstract*—Efficient mode division multiplexing using the spatial aperture sampled concept from single-modefibers to a few-mode fiber is extended to circular step index fibers supporting up to ten spatial modes and to annular refractive index profile fibers supporting nine optical orbital angular momentum modes (mode counts double when considering polarization states for each case). Each sampling beam aperture is spatially shaped for lower average coupling losses and mode dependent losses or a balance thereof. The optimization demonstrates the scalability and consistent low losses for the aperture-sampled mode multiplexer for increasing mode counts, as opposed to the phase hologram-based mode conversion technique. The aperture-sampling approach is also found to be robust to small input fiber alignment errors and fiber geometrical distortions.**

***Index Terms*—Fiber optics, fiber optics communications, multiplexing.**

I. Introduction

THE incessantly increasing data volume that optical networks are transporting implies that within a few years we may reach the maximal attainable capacity over a single mode fiber (SMF) for typical transmission range of hundreds of kilometers. Space-division multiplexing (SDM) [1] has been attracting great attention recently [2]–[6], as a means to overcome the transmission capacity exhaust of SMF by introducing additional conduits of information. SDM is possible through the use of multi core fibers [7] or multimode fibers guiding limited number of spatial modes (few mode fibers (FMFs)). Implementing SDM with FMFs, can advantageously provide a capacity boost without a fiber count or guiding core number increase.

There are several technological barriers before mode-division multiplexing (MDM) can be adopted, one of which is the efficient multiplexing into, and demultiplexing out of, a FMF. The (de)multiplexer design should be optimized to offer low optical losses for interfacing to FMF and minimize mode dependent loss (MDL). MDL occurs when the multiplexer exhibits uneven losses per spatial mode, hence modal information loss arises [20]. Spatial mode conversion [2]–[5], the straightforward way for MDM, loses overall multiplexing efficiency due to the requisite power splitting/combining process; thus overall high insertion losses (IL) are undesirably obtained. Its main advantage is that modal information is not mixed by the multiplexing operation. The spatial aperture-sampling mode multiplexer/demultiplexer uses an alternative method which eliminates the need for the splitter/combiner and its associated losses. The basic operating principle of this demultiplexer is the sampling of the FMF aperture instead of the conversion of each mode. By sampling the FMF facet, all guided modes are coupled to an SMF array, each mode coupling with finite efficiency to each aperture. This scheme does result in strong mixing between the modes, which if performed throughout the communication link can advantageously lead to statistically narrow spread of differential group delays (DGD) between the modes [6].

One arrangement for this demultiplexer utilizes adiabatic tapering down of a SMF bundle until coupling between the vanishing cores begins and forms supermodes that match the FMF aperture, a device often called "photonic lantern" [8]. Photonic lanterns were first introduced in the field of astrophysics [9], [10], and were subsequently adopted for optical communication [11], [13], [14]. Multiplexing through photonic lanterns can be lossless and MDL free in theory, but suffers from the sensitivity disadvantages of the adiabatic process in practice [11]. Recently a mode preserving three mode photonic lantern multiplexer was introduced [10]–[12], but still needs to be demonstrated in order to prove it can scale to high mode counts.

Alternatively, the individual apertures can be abruptly coupled to the FMF by free-space imaging or direct contact. The free space imaging approach has been demonstrated for a three mode fiber [14], [15]. In the abrupt coupling approach, the individual beams of the multiple input SMF sources are mapped onto distinct locations within the FMF core. Each SMF image serves as an independent source and illuminates a finite aperture of the fiber face, hence couples with fixed efficiency to each linearly polarized (LP_{nm}) mode of the FMF (see Fig. 1), where *n* and *m* are the azimuthal and radial orders, respectively. Each aperture, φ_i, contributes to the excitation of the j'th supported mode, by evaluating the overlap integral, and the coupling values, ξ_{ij}, can be assembled to the mapping matrix form:

$$\begin{pmatrix} \mathrm{LP}_{01} \\ \mathrm{LP}_{11v} \\ \mathrm{LP}_{11h} \\ \cdots \end{pmatrix} = \begin{pmatrix} \xi_{11} & \xi_{12} & \xi_{13} & .. \\ \xi_{21} & \xi_{22} & \xi_{23} & .. \\ \xi_{31} & \xi_{32} & \xi_{33} & .. \\ .. & .. & .. & \cdots \end{pmatrix} \begin{pmatrix} \varphi_1 \\ \varphi_2 \\ \varphi_3 \\ \cdots \end{pmatrix}. \quad (1)$$

The mapping matrix from apertures to modes, ξ, describing the multiplexing operation can be conjugate transposed, ξ^*, thereby describing the mapping from modes to apertures. The cumulative effect of multiplexing and demultiplexing (neglecting mode mixing in transmission fiber) can therefore be described by the matrix operation $\xi^*\xi$. If the mapping operation ξ is orthogonal, then the matrix product $\xi^*\xi$ is the identity matrix

Manuscript received September 7, 2014; revised February 15, 2015 and April 25, 2015; accepted May 26, 2015. Date of publication June 23, 2015; date of current version November 1, 2015.

The authors are with the Applied Physics Department, Hebrew University, Jerusalem 91904, Israel (e-mail: miri.blau@mail.huji.ac.il; danmarom@mail.huji.ac.il).

Color versions of one or more of the figures in this paper are available online at http://ieeexplore.ieee.org.

Digital Object Identifier 10.1109/JLT.2015.2449333

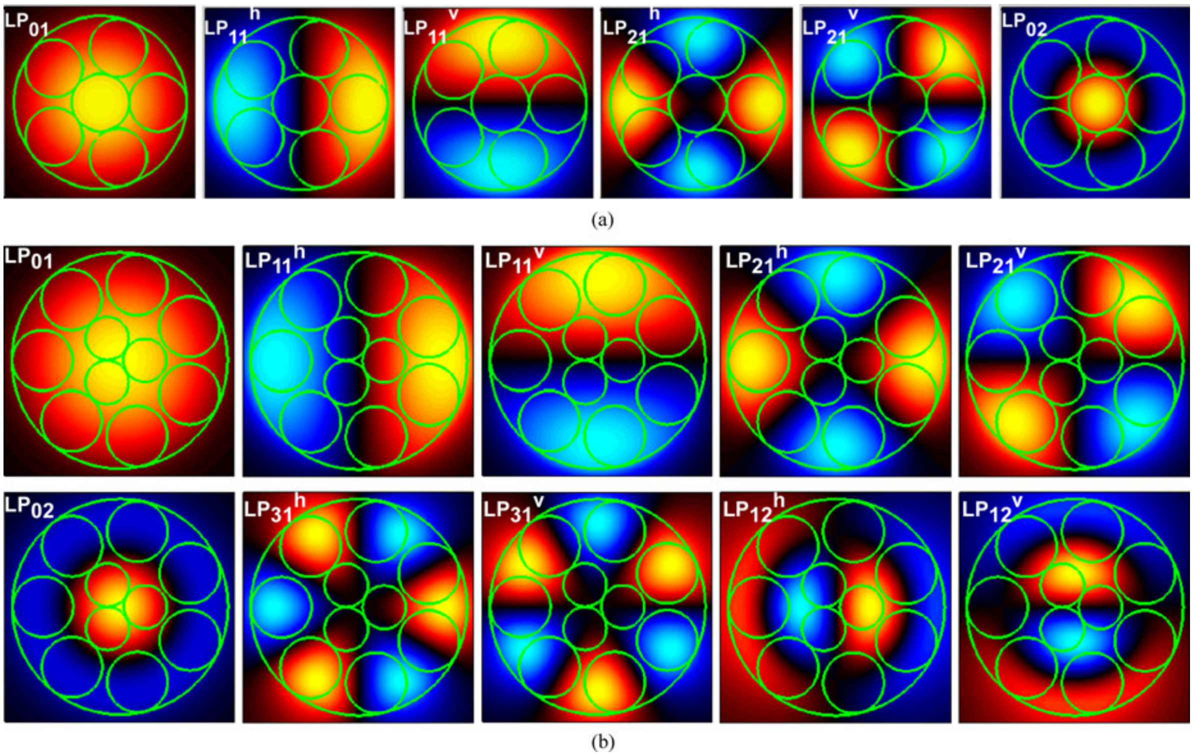

Fig. 1. Field distribution of LP_{nm} modes of a step index fiber: core and location of circular aperture outlined in green. Top: Six mode fiber. Bottom: Ten mode fiber.

and all information is preserved, and readily available for detection. In practice, modes mix throughout transmission in a FMF, hence the recovered signal is $\xi^* \boldsymbol{A} \xi$, where $\boldsymbol{A}$ describes the modal mixing operation which ideally is a unitary transformation. The recovered signal at each demultiplexer SMF output contains a superimposed signal of all modes with different time-varying amplitudes, phases, and differential time delays, as a result of the mixing matrix $\boldsymbol{A}$. Since all involved matrices are ideally unitary, the information can still be recovered from the received demultiplexed channels after coherent detection, with the aid of MIMO (multiple input, multiple output) processing which attempts to invert the modal mixing matrix A [16].

Thus the key requirement for the mapping from sampled modes to individual apertures is that the mapping vectors be orthogonal. The number of spatial samples should be identical to the propagating mode count, thereby matching the ranks of the two spaces. The adiabatic transition of the photonic lantern has been shown through simulation to fulfill this requirement using the beam propagation method [23]. With the abrupt transition techniques, incomplete energy transfer in the mapping results in losses. Had these losses been uniform for all modes, implying mapping vectors are still orthogonal but of magnitude less than unity, then the $\xi^* \xi$ product would still be a diagonal matrix with a constant value less than one on its main diagonal. Such uniform losses represent no modal loss of information (since the diagonal elements are identical) and the MIMO processing can still recover the original signal, subject to detection SNR. Nonuniform efficiency for mode mapping vectors results in different trace elements in $\xi^* \xi$, which translate into mode-dependent performance degradation quantified by the MDL metric [17]. Hence, the design goal of the spatial aperture sampling multiplexer is to define the apertures such that the mapping vectors are as close to orthogonal, with minimal losses and high uniformity.

In SMF systems, which support two orthogonal polarization states, components are specified by their loss performance difference, denoted polarization dependent loss, which is defined as the power ratio of the two trace elements of the component's Jones transfer matrix. With the advent of SDM, component MDL is quantified by the power ratio between the least and the most attenuated states in the hyperpolarization space (consisting of all supported spatial and polarization modes). The component MDL metric measures the extreme performance bounds. For SDM communication systems that experience random coupling in transmission and traverse multiple components, thereby accumulating MDL, an alternative MDL definition that measures the standard deviation of the trace elements is more useful for predicting the accumulated MDL [17], [19]–[22]. As such, overall system MDL grows linearly in a transmission system, taking into account the components' standard deviation MDL metric. In this paper we quantify the performance using the conventional definition of MDL (max-min ratio), for consistency with previous papers and as a predictor of worst case scenario.

In our previous work [18], we introduced the optimization of the spatial aperture sampling multiplexer for a three mode step index fiber. By introducing shaped aperture geometries, 11% greater efficiency than that of the simple circular Gaussian was achieved, with MDL of less than 0.2 dB. However, the adoption of new transmission fiber requires extensive

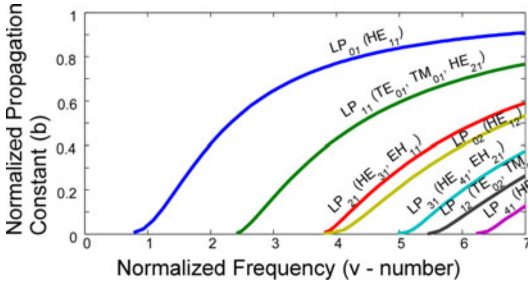

Fig. 2. Dispersion curves of LP modes in step index fibers.

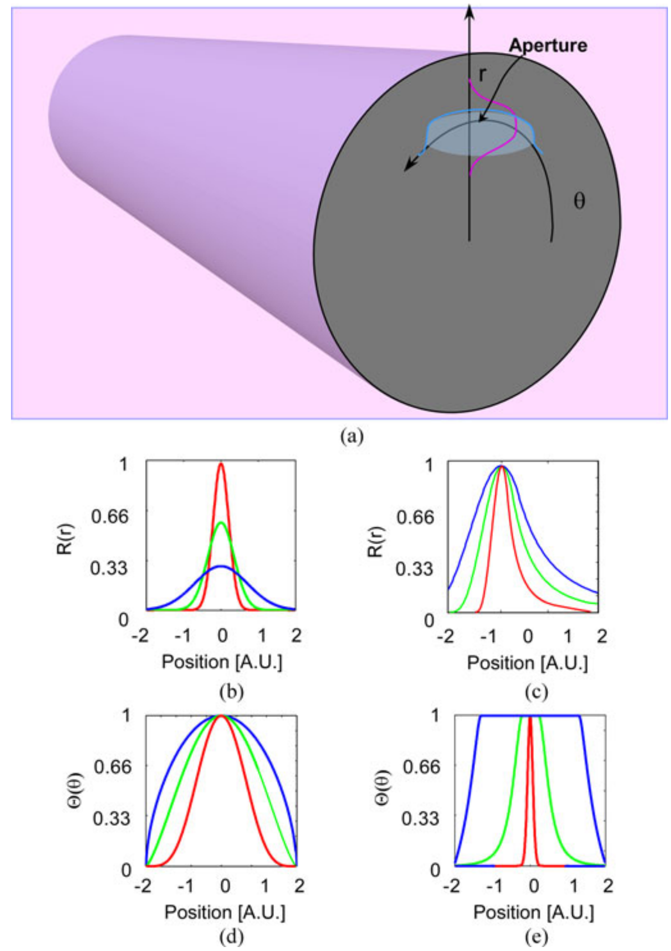

Fig. 3. (a) Illustration of aperture constructed by radial and azimuthal functions. (b)–(e): The different radial and azimuthal aperture functions, with varying parameters. (b) Gaussian function, (c) Radial Bessel function, (d) Azimuthal cosine raised to the power, (e) Azimuthal adjustable raised cosine function.

changes to the whole optical communications infrastructure, and such changes have to provide a significant increase in capacity at an incremental cost structure, such that the overall cost-per-bit is significantly reduced [19], [20]. Complete new infrastructure would probably make economic sense if at least an order of magnitude greater capacity (mode count) is offered. In this paper we show the scalability of the spatial sampled aperture method by applying it to high mode count and different refractive index profile fibers. In both cases we find improved efficiency of coupling when comparing to the circular Gaussian aperture sampling. We expand the aperture sampling approach using shaped apertures to efficiently multiplex into a step index fiber supporting six and ten spatial modes, as well as annular refractive index profile fiber supporting nine orbital angular momentum (OAM) modes. We demonstrate that the advantages of shape-optimizing the apertures continue and the overall mapping losses increase only moderately for higher mode counts. However, the technique does not yield simultaneously minimal average IL and low MDL, but one metric can be minimized at the expense of the other.

II. Spatial Sampling Multiplexer Optimization for a FMF

The spatial aperture sampling mode multiplexer's efficiency strongly depends on the apertures' shape, arrangement and size. An optimization process is a necessary step even when considering basic circular Gaussian apertures [15], [23], [24]. The location of the apertures, their size and shape, have a significant influence on the average coupling IL and MDL. An optimized shaped aperture is one that leads to low average IL and low MDL by well matching the spatial modal structure, while distinguishing between all modes.

The *size* parameter is optimized by computational sequential search; its basic goal is to minimize energy loss by good coverage of the fiber's facet while avoiding overlap of the apertures. The *arrangemen***t** parameter is also important for the same reasons, but has one more requirement: as degenerate modes (e.g., $\mathrm{LP}_{11}^{a}, \mathrm{LP}_{11}^{b}$) are identical except their azimuthal orientation, the arrangement must be asymmetric in order to distinguish between them. Setting the apertures' arrangement in $m-1$ concentric circles, with $2n+1$ elements equally spaced along the outer circle, satisfies this requirement, where the *n, m* values are those of the highest supported spatial mode. In the six mode fiber (supporting LP_{01}, LP_{11}, LP_{02}, and LP_{21}, as shown in Fig. 1(a)), the normalized frequency is of $2.40 < \mathrm{V} < 3.83$ (see Fig. 2). This corresponds to having the apertures distributed along two rings, five apertures on the outer circle and a single additional aperture in the inner circle (which has zero radius). In the ten mode fiber (with additional support of LP_{12} and LP_{31}, as shown in Fig. 1(b), and normalized frequency region extended to $3.83 < \mathrm{V} < 5.21$), seven apertures are placed on the outer circle and three on the inner circle. In all cases the number of apertures equals the number of supported modes (to match mode and aperture spaces) and orthogonality between the apertures is maintained through judicious placement and sizing of the apertures, in order to best preserve the information for subsequent electronic MIMO processing.

The last parameter is the *shape* of the apertures. As we demonstrated in our previous work [18], the aperture shapes we considered for optimization are: (a) circular Gaussian, (b) elliptical Gaussian, (c) raised cosine, and (d) cosine raised to power *x* (see Fig. 3). The circular Gaussian case is used as a benchmark for comparing against the SMF imaging case [24]. The elliptical Gaussian case adds eccentricity to the apertures, which allows for better coverage of the FMF aperture. The degrees of freedom of a circular Gaussian aperture are its radius and position (see Fig. 3(a)). For elliptical Gaussian aperture, the axes for the radial and azimuthal directions can be independently set, with the

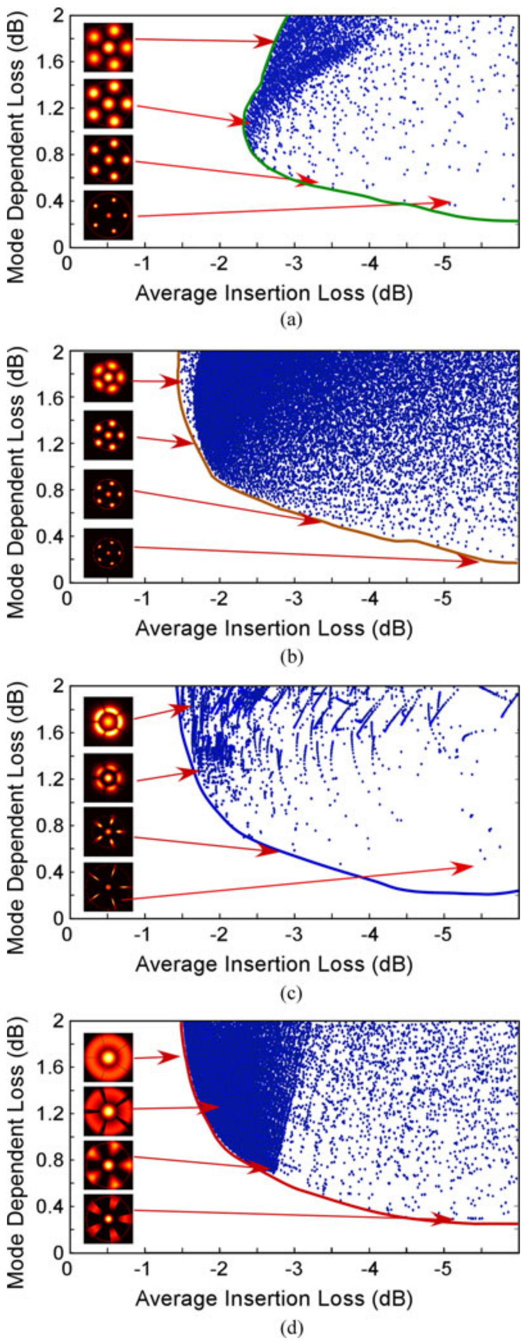

Fig. 4. Aperture optimization results for a six mode fiber. MDL as a function of IL for various geometries. Intensity pattern distributions for minimal MDL and IL values. (a) Circular Gaussian apertures. (b) Elliptical Gaussian apertures. (c) Radial Bessel function and azimuthal raised cosine function apertures. (d) Radial Bessel function and azimuthal cosine raised to the power x ($x < 1$) dependency apertures.

major and minor axis coinciding with the radial and azimuthal orientations.

To gain greater freedom in aperture realization, we further consider specifying the aperture using separate functions for the azimuthal and radial directions. Each combination of radial and azimuthal functions form together a specific aperture shape. For the azimuthal distribution function, $\Theta(\theta)$, the raised cosine function and cosine raised to power x shapes were used.

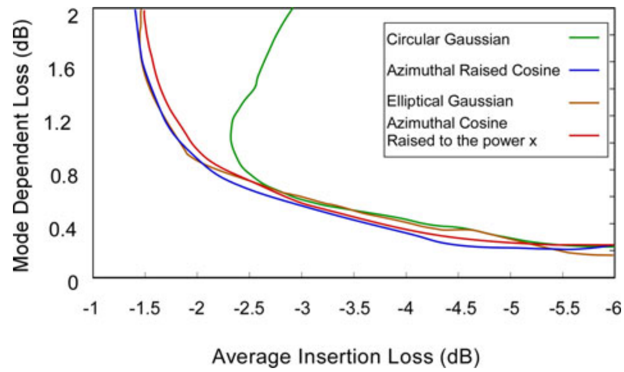

Fig. 5. Performance leading edges of MDL versus IL values for all optimized aperture geometries for a six mode step index fiber.

For the radial distribution function, $R(r)$, we chose a functional form based on Bessel functions, which well matches the fiber's modes. This radial Bessel functional form was defined by:

$$R(r) = \begin{cases} J_n(\alpha(r+\rho)), & r_0 < r \le r_1 \\ A \cdot K_n(\beta(r+\rho)), & r > r_1 \end{cases}. \tag{2}$$

A few variations of the radial Bessel function forms are presented in Fig. 3(b). The functional variations depend on the radial position parameter, ρ, the scaling parameter of the function, α, the Bessel index n, and the radii values r_0 and r_1 (which are dependent variables resulting from the position and scaling degrees of freedom). The normalization constants A and β are also dependent variables, and cannot be used as additional degrees of freedom; they serve to ensure the function is continuous. The azimuthal functional form for the cosine raised to power x was

$$\Theta(\theta) = \cos^x\left(\frac{(2n+1)\,\theta}{2}\right) \; |\theta| < \frac{\pi}{2n+1} \tag{3}$$

where n is the maximal azimuthal order supported by the FMF (2 and 3 for the six and ten modes, respectively). The aperture spans an angular range of $\pm\pi/(2n+1)$, and raised to a variable power x which is the only optimization parameter (see Fig. 3(c)). The functional form for the raised cosine was

$$\Theta(\theta) = \begin{cases} 1, & |\theta| \le \beta \\ 0.5\left[1+\cos\left(\frac{(2n+1)}{\pi-(2n+1)\beta}(|\theta|-\beta)\right)\right], & \beta < |\theta| \le m \le \frac{\pi}{2n+1} \end{cases} \tag{4}$$

again forming $2n+1$ separate azimuthal spots. The adjustable raised cosine function is described by two parameters; m, which determines the point where the sinusoidal part of the function begins and as a result the width of the non-zero angular section, and the parameter β sets the transition width from zero to one of (see Fig. 3(d)).

An optimized shaped aperture achieves low average IL and MDL. Each aperture is optimized using the degrees of freedom associated with it. For example, in a ten mode fiber and the raised cosine apertures, the center aperture size parameter is replaced by two radial degrees of freedom (function scaling and degree of

Bessel function) and two azimuthal (β and m), in addition to the phase rotation between the internal and the external apertures. The outer apertures also possess four degrees of freedom (two azimuthal and two radial) along with the displacement degree of freedom, for a total of ten degrees of freedom. In the same case of a ten mode fiber, the circular Gaussian apertures introduces five degrees of freedom: internal circle aperture radius and displacement, external circle aperture radius and displacement and the phase rotation between the internal and external circles of apertures.

We exhaustively searched across all aperture variations for each aperture shape considered, varying all parameters to manipulate the apertures' shapes in order to obtain best coupling. As we deal with a large number of degrees of freedom, we chose to present our optimization results as MDL versus IL scatter plots, where each point represents a specific geometric realization (determined by the parameters chosen), and demonstrate the general trend of aperture shape change in a few specific cases (Figs 4, 6, 12). This scatter plot defines the 'accessible optimization area', the MDL and IL values that are realizable using the specific aperture form in the system described above. Each 'accessible optimization area' is further defined by its 'leading performance edge'—the outline of the scatter graph achieving best MDL-IL pairs.

In our optimization process we seek a geometry which will provide zero MDL and minimal average IL, converging to the lower left corner in our scatter plot. However, we find the minimal IL results in an elevated MDL (top left corner) and minimal MDL in elevated IL (bottom right corner). As expected, there is an increasing average IL trend as the mode count increases, although quite moderately. MDL is also elevated when mode count increases: for a ten mode fiber, MDL <0.5 dB will be obtained with higher average IL than that of MDL <0.5 dB in the six mode fiber case. This is attributed to the more elaborate spatial variations for higher modes.

III. Spatial Sampling Multiplexer Optimization for a Step Index Fiber

We propose an optimization method for an aperture sampling mode MUX/DEMUX. We chose to use a step index fiber in our simulations, as a universally accepted fiber appropriate for demonstration of our method. Naturally, each specific fiber design, specified by its geometry and refractive index distribution, will require its own optimization process according to the refractive profile fiber specifications. (The same is true for the photonic lantern based mode mux/demux). Our optimization process is based on two different optimization parameters, average IL and MDL, which led us to investigate the relationship between them. As can be seen in Fig. 4, a negligibly small MDL is obtained when the apertures are small, so the coupling into each mode is reduced to the point where they are nearly uniform across all modes. When looking for the best IL, wide apertures which significantly overlap with most modes emerge. The wider apertures have higher IL values for modes with fine structures (high m,n values), leading to MDL. Aperture optimization results for the six mode fiber are shown in Fig. 4. In Fig. 5 we

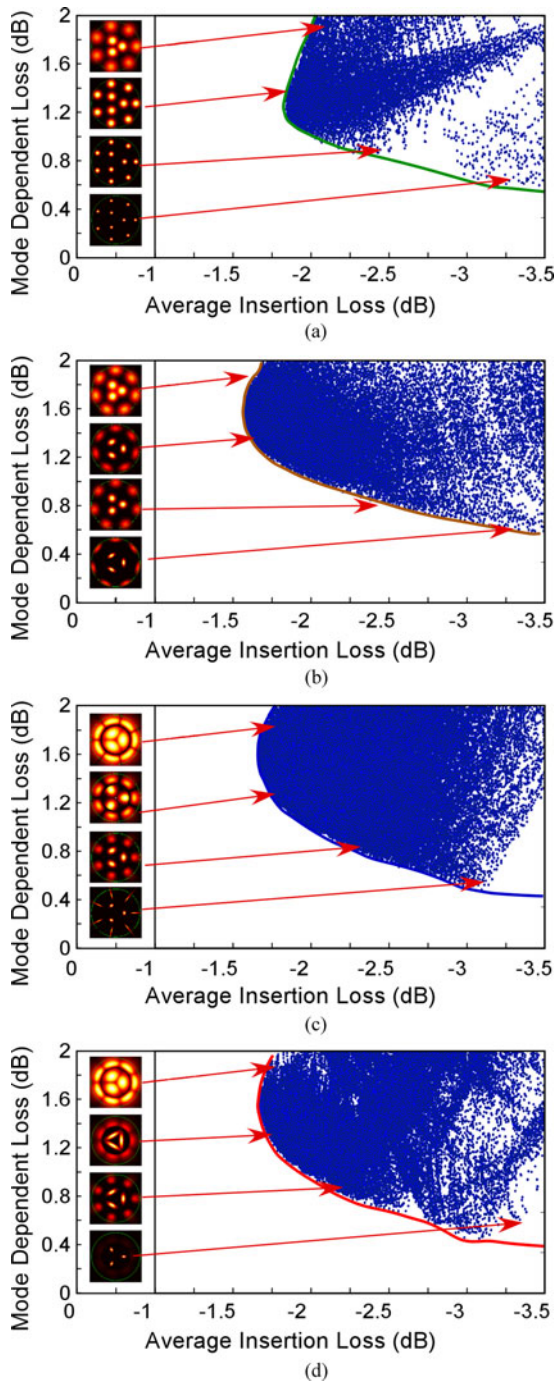

Fig. 6. Aperture optimization results for a ten mode fiber. MDLs as a function of IL for various geometries. Intensity pattern distributions for minimal MDLs and IL values. (a) Circular Gaussian apertures. (b) Elliptical Gaussian apertures. (c) Radial Bessel function and azimuthal raised cosine function apertures. (d) Radial Bessel function and azimuthal cosine raised to the power x ($x < 1$) dependency aperture.

show the leading performance edges of the accessible optimization areas of the various apertures, setting the minimal MDL and IL values for each option.

This way a comparison between the accessible optimization spaces of the different aperture geometries is presented, allowing for a better comparison. As can be seen in Fig. 5, the optimization accessible area when using the circular Gaussian apertures

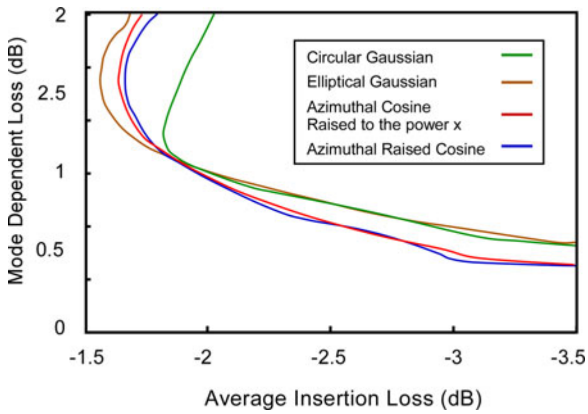

Fig. 7. Performance leading edges of MDL versus IL values for all optimized aperture geometries for a ten mode step index fiber.

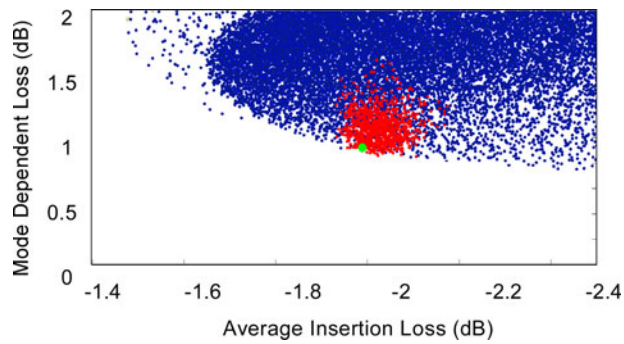

Fig. 8. Efficiency sensitivity to location errors of elliptical Gaussian apertures for a six mode fiber. Blue points: IL-MDL values of different aperture realizations; Green point: Selected optimization value; Red points: IL-MDL variations due to randomly mislocated apertures.

is much smaller than that of the other apertures' shapes. For a very low MDL target (MDL→0), i.e., by generating small enough apertures, the circular Gaussian apertures will perform as well as the other aperture shapes. However, low average IL requires the efficient power collection over the FMF facet, and tightly packed circular Gaussian apertures do not efficiently span a circular aperture. Our theoretical results can be compared to recently reported experimental results [24], where multiplexing in and demultiplexing out of a six mode fiber was reported, with IL < 6 dB for each mux/demux, and an MDL value of 4.5 dB for the entire system.

We next extend the optimization of the spatial aperture sampling demultiplexer when more LP modes are guided in the FMF by simulation of a ten mode fiber (see Fig. 1(b)). As before, after examining the simple circular Gaussian beam case, we optimized the apertures' shape using functions (2)–(4). Aperture optimization results for the ten mode fiber are shown in Figs. 6 and 7.

The trend of increasing IL with higher guided mode count continues, but unlike the phase hologram- based mode conversion technique, the spatial aperture sampler's IL increases slowly. For the ten mode fiber we can obtain an insertion loss of less than -1.65 dB (see Fig. 6(b)), where passive combining loss alone for the mode conversion multiplexer is -10 dB. As previously explained, lower MDL can be obtained at higher IL values.

As fiber positioning and alignment is always limited in accuracy, a sensitivity simulation of the coupling efficiency as a result of SMF alignment errors was carried out. Fig. 8 shows the Monte Carlo simulation of the effect of fiber placement error, by introducing independent errors for each SMF input (normally distributed, with 90% of alignment errors within ± 0.5 μm). The FMF designed core radius is 9 μm and the apertures' intended radii are 2.75 μm for the central aperture and 3.5 μm for the outer apertures.

The design starting point is shown in green (IL $= -1.98$ dB, MDL $= 0.92$ dB) and the 1000 trial simulation generates a red cloud about it, showing the resulting IL and MDL values obtained when each aperture of the six is slightly misplaced. More than 90% of the displaced apertures have an IL within ± 0.12 dB of the design value and the excess MDL range is 0.3 dB. Misalignment can also impact orthogonality of the projections vectors: If the misalignment is large enough to cause overlap between two or more apertures the orthogonality will decrease. However, for small enough misalignment, the apertures will probably not cross over and small damage to the orthogonality will be caused. Accordingly, simulation showed less than 50 deviation from perfect orthogonality (by measuring the angles between the projection vectors).

The optimization process for high mode counts and aperture degrees of freedom can quickly escalate to an intractable problem. An exhaustive search of the whole optimization area can be done at coarse sampling resolution or alternatively endure very long calculation times, so a more directed search is required. A few simple guidelines are offered for a directed search: First the aperture arrangement over the fiber's facet has to match the mode pattern. As can be seen in Fig. 1(b), the higher radial order modes form two rings of intensity, and the apertures' arrangement form two circles. The confinement of the guided modes within the core decreases for higher modes, and in order to match this pattern the outer apertures should extend beyond the core's edge, such that some of the cladding area is encapsulated by the outer apertures. The diameter of the inner circle of apertures should be in the area of the inner ring of intensity. For a fiber guiding more modes, the intensity pattern consists of more intensity rings and additional circles of apertures will be needed. These additional circles will be optimized in the area of the diameter of the matching intensity ring, as described above. When optimizing for best IL, the apertures should collect as much intensity as possible, resulting in large apertures. When optimizing for minimal MDL the trend is opposite, leading to point-like apertures where there is little benefit in customized aperture shapes.

IV. Spatial Sampling Mode Multiplexer Optimization for a Nine Mode Annular Fiber

The spatial aperture sampling approach can be applied to any refractive index profile fiber. Here we demonstrate this for a more exotic refractive index profile of a step index annular fiber. An annular fiber has an internal and external cladding region (we assume here of equal refractive index, but this is not

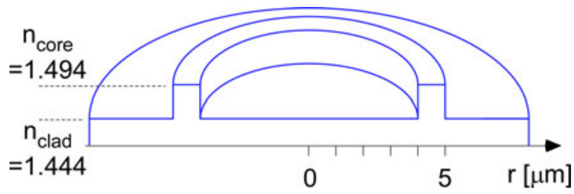

Fig. 9. Refractive index profile of an annular fiber.

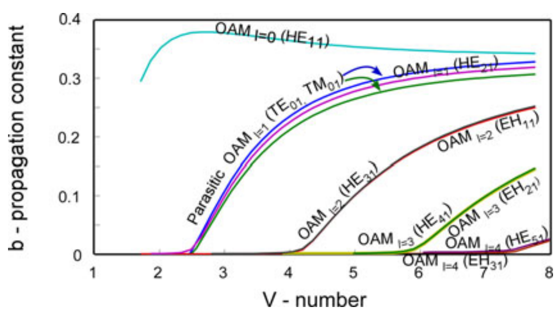

Fig. 10. Dispersion curve of OAM modes in annular index fibers with single radial mode.

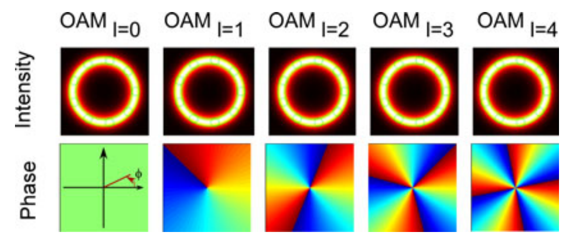

Fig. 11. Intensity and phase patterns of the propagating modes in a nine mode annular fiber. Sampling apertures outlined in green. The negative momentum modes (not shown), OAM l = 0 through OAM l = 4 have an opposite phase gradient.

mandatory), with an annular core of higher index residing in between, as shown in Fig. 9. When analytically solving Maxwell's equations using the boundary conditions of the annular fiber, we obtain the vector modes TE, TM and hybrid (HE and EH) modes, as in the step index fiber. Each hybrid mode supports two orthogonally polarized modes, as in step index round core fibers. In low index contrast step index fibers we can convert the vector modes into linearly polarized (LP) mode groups by adding and subtracting vector modes with close propagation constant. As LP modes propagate in the fiber, each of the fiber's vector modes propagates in a slightly different propagation constant as described in detail in [25]. In annular fiber we can convert the vector modes to OAM modes [26], defined by adding and subtracting the two twofold degenerate hybrid modes with a $\pm\pi/2$ temporal phase shift [25]–[30]. Since degenerate modes are combined, their propagation constants are identical and hence the OAM modes should be better preserved in propagation. Note that the TE_{01} and TM_{01} can also be added and subtracted with a phase delay and generate a linear azimuthal phase, but since these vector modes have slightly different propagation constants they do not form a stable OAM mode (sometimes referred to as the parasitic OAM mode). OAM modes are of constant azimuthal intensity, a circular polarization state of either clockwise or counter-clockwise (CW and CCW), and a linearly varying phase along the azimuth (see Fig. 11). Hence, OAM modes are simply another orthogonal basis to represent the vector modes of the optical fiber. Indeed, recent research has shown the capability of OAM excitation and transmission in fiber [26]–[33]. To fully benefit from the stability of OAM modes, each information channel has to be mapped to an OAM mode, which is similar to the role of a mode-conversion multiplexer. This can be achieved by a spot-based multiplexer with proper phase relationship and polarization preparation [29]–[32].

The aperture sampling mode multiplexer can be applied and optimized for the annular fiber. Prior to optimizing the multiplexer operation, we mathematically solve dispersion equation and obtain the supported vector modes (see Fig. 10). Our annular fiber model is based on a step index profile with a constant guiding thickness designed to support a single radial mode; we vary the outer radius and observe additional azimuthal guided mode solutions as the circumference increases. When the external radius is less than the annulus width, the fiber is effectively a step index fiber. As the outer radius increases the annular structure becomes prominent; hence the fundamental mode initially behaves as a step index fiber (rising monotonously) and then reduces and converges to the fundamental annular mode $\mathrm{OAM}_{l=0}$ with no cutoff frequency. The diameter defines the number of azimuthal modes, *N*, which determines the number of sampling apertures. OAM modes are degenerate in their phase gradient direction (sign of *l*) except for the basic OAM_0 mode (see Fig. 10), therefore the highest azimuthal index propagating in the fiber, *l*, determines the aperture count according to $N = 2l + 1$. Under these conditions, when *N* coherent inputs of the same power and CW or CCW polarization have the phase relationship of $\Delta\Phi = \Phi_n - \Phi_{n-1} = 2\pi l/N$, a pure OAM_l mode will be generated [26]. In our simulation we used a nine mode annular fiber, i.e., $l = 4$.

We apply the spatial aperture sampled multiplexing process to the annular fiber, in a very similar process described before for a step index FMF. Each source excites all modes to a certain degree and from the coupling matrix the modal properties of IL and MDL are derived. If an additional optical processing block is introduced to convert each mode to span all spots with the proper phase and polarization in a unitary fashion, then the information would be mapped to OAM modes. When optimizing the multiplexer for an annular fiber we first used the two basic apertures: circular Gaussian and elliptical Gaussian. When moving on to the separable functions, we used the exact radial profile of the fiber's fundamental mode (found by analytically solving for the propagating mode profiles), consisting of Bessel functions of different types in the core and cladding regions. This leaves us with only two degrees of freedom for of the azimuthal functions as defined by Eqns. (2) and (3). Aperture optimization results for the nine mode ring fiber are shown in Figs. 12 and 13. Again we see that the circular Gaussian apertures suffer from higher IL and MDL than that of the differently shaped apertures.

In the process of fiber pulling a small degree of ellipticity of the fiber can occur. We next tested the stability of the optimization process with 0.1%–2% fiber ellipticity (see Fig. 14). MDL

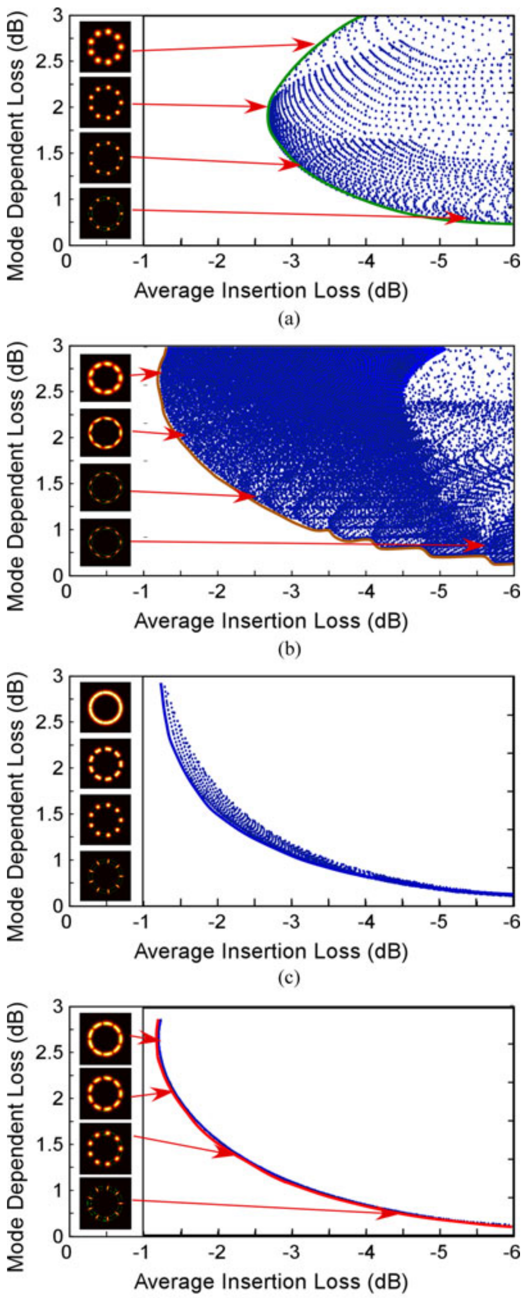

Fig. 12. Aperture optimization results for a nine mode ring fiber. MDL as a function of IL for various geometries. Intensity pattern distributions for minimal MDL and IL values. (a) Circular Gaussian apertures. (b) Elliptical Gaussian apertures. (c) Ring fiber mode radial function and azimuthal raised cosfigine function apertures. (d) Ring fiber mode radial function and azimuthal cosine raised to the power x ($x < 1$) dependency apertures.

and IL sensitivity to 2% ellipticity results in ∼0.05 dB degradation in MDL and <0.1 dB in IL, thus proving low sensitivity to ellipticity of the fiber.

V. Step Index Fiber Versus Annular Fiber

After optimizing sampling apertures for both step index fiber and annular fiber, we can now compare them (see Fig. 15). Although the two fibers support nearly the same number of modes (nine for the annular fiber and ten for the step index fiber), it is evident that the annular fiber performs better than the step index fiber for multiplexer metrics of IL and MDL. This is due to the less intricate mode distributions in an annular fiber, when designed to support a single radial order.

Other factors, beyond multiplexer performance, may influence the fiber design choice. If modes mix, whether at the multiplexer or in transmission, then MIMO processing is necessary at the receiver. In order to minimize the time domain range of the MIMO processing it is highly desirable to reduce the DGD between the modes in each fiber. This usually entails having a more gradient phase profile than the step index used throughout this paper. However, the same optimization procedures still

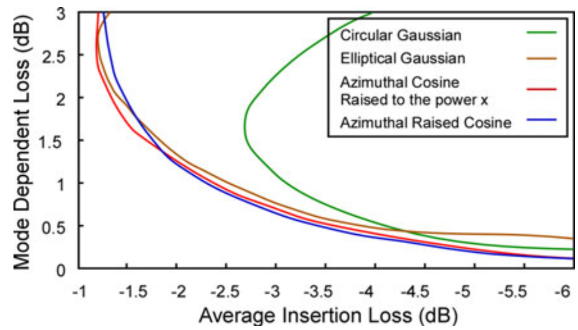

Fig. 13. Performance leading edges of MDL versus IL values for all optimized aperture geometries for a nine mode annular fiber.

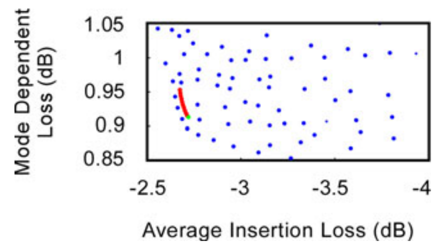

Fig. 14. Efficiency sensitivity to ellipticity of an annular fiber. Blue points: IL-MDL values of perfectly circular fiber; Red point: Selected optimization value; Green points: IL-MDL variations due to randomly ellipticity values of the fiber.

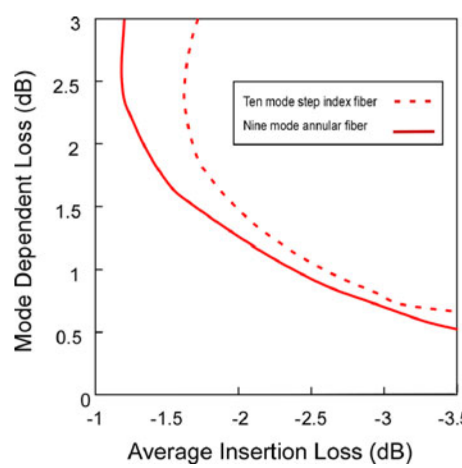

Fig. 15. Optimization area of ten mode step index fiber and nine mode annular fiber.

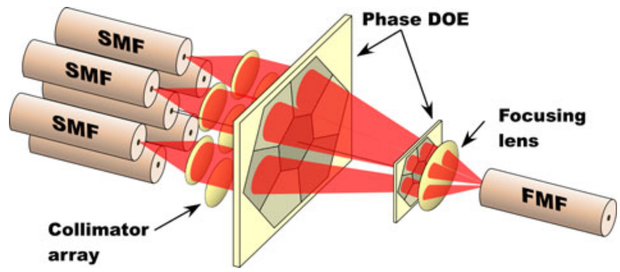

Fig. 16. Realization scheme proposal for a six mode multiplexer.

apply and the annular fiber should continue and outperform the graded index round core fiber. Note that in graded index round core fiber the number of degenerate modes in higher mode groups increases rapidly and hence the main mode coupling in transmission, being within a degenerate mode group, now encompasses more modes. In an annular fiber, even after refractive index distribution optimization, the number of modes in each OAM mode group (modes with the same angular frequency) remains fixed at four, except for the case $l = 0$, where the number of modes in the OAM mode groups is only two. This may be advantageous for MIMO processing, especially if mode coupling between mode groups is low and a mode preserving multiplexer is employed.

VI. Suggested Realization Schemes

Generating the spatial beam distributions described by functional forms of Eqs. (2)–(4) is possible with the use of two phase-only diffractive optical elements (DOE) placed in cascade (see Fig. 16), where the first DOE controls the amplitude distribution at the plane of the second DOE via diffraction, and the latter corrects the phase distribution to achieve efficient coupling into the FMF [34], [35]. By employing phase-only DOE encoding, theoretically efficient diffraction efficiency may be achieved, reducing the additional IL of the multiplexer to a minimum [36], [37]. The aperture functions we chose define smooth and continuous distributions, allowing both DOEs to be encoded with slowly varying and moderate phase depths, which will yield efficient diffractive realizations. Since the intent is to slightly change the distribution in each case (from circular to elliptical or related forms), and all shape functions result in generally similar apertures, the functional form will resemble roughly elliptical lens, or crossing of two cylindrical lenses. Anti-reflection coating can further reduce the Fresnel reflections and help achieve low loss attributes. Since the phase encoding functions are moderately varying, it is possible to implement the same beam shaping approach with refractive optical elements, as described in [38].

VII. Conclusion

We demonstrated the scaling potential of the spatial aperture sampled mode multiplexer for large number of modes and various refractive index fiber profiles, and its performance degradation due to misalignment. Optimizing the beam shapes beyond circular Gaussian expands the accessible optimization space, and allows one to achieve lower average IL. In the optimization process a negligibly small MDL can be obtained for all geometries, but at higher average IL values using point-like sampling apertures. In this scenario, there is little benefit in exploring specialized apertures. When optimizing for minimal IL values, the shaped apertures achieve better results as they can better envelope the core aperture. The same characteristics are found for an annular fiber supporting OAM modes. When optimizing for an acceptable MDL level, the shaping results in lower IL. Guidelines for the optimization for high mode count fibers were offered, by matching aperture arrangement and spreading over the fiber's facet to spatial mode pattern. In order to prevent loss of channels and as a result, information loss, the symmetry of the mode pattern should be noticed. Since the losses of the spatial aperture sampling multiplexer/demultiplexer increase very moderately with higher mode counts, the optimized multiplexer is suitable for interfacing to fibers guiding tens of spatial modes.

References

[1] S. Berdagué and P. Facq, "Mode division multiplexing in optical fibers," *Appl. Opt.*, vol. 21, pp. 1950–1955, 1982.
[2] R. Ryf, S. Randel, A. H. Gnauck, C. Bolle, R. Essiambre, P. Winzer, D. W. Peckham, A. McCurdy, and R. Lingle, "Space-division multiplexing over 10 km of three-mode fiber using coherent 6 × 6 MIMO processing," presented at the Optical Fiber Communication Conf. Expo./Nat. Fiber Optic Engineers Conf., Los Angeles, CA, USA, 2011, Paper PDPB10.
[3] S. Randel, R. Ryf, A. Sierra, P. J. Winzer, A. H. Gnauck, C. A. Bolle, R.-J. Essiambre, D. W. Peckham, A. McCurdy, and R. Lingle, "6 × 56-Gb/s mode-division multiplexed transmission over 33-km few-mode fiber enabled by 6 × 6 MIMO equalization," *Opt. Express*, vol. 19, pp. 16697–16707, 2011.
[4] M. Salsi, C. Koebele, D. Sperti, P. Tran, P. Brindel, H. Mardoyan, S. Bigo, A. Boutin, F. Verluise, P. Sillard, M. Bigot-Astruc, L. Provost, F. Cerou, and G. Charlet, "Transmission at 2x100 Gb/s, over two modes of 40 km-long prototype few-mode fiber, using LCOS based mode multiplexer and demultiplexer," presented at the Optical Fiber Communication Conf. Expo./Nat. Fiber Optic Engineers Conf., Los Angeles, CA, USA, 2011, Paper PDPB9.
[5] J. von Hoyningen-Huene, R. Ryf, and P. Winzer, "LCoS-based mode shaper for few-mode fiber," *Opt. Express*, vol. 21, pp. 18097–18110, 2013.
[6] S. Ö. Arık, D. Askarov, and J. M. Kahn, "Effect of mode coupling on signal processing complexity in mode-division multiplexing," *J. Lightw. Technol.*, vol. 31, no. 3, pp. 423–431, Feb. 2013.
[7] C. Xia, N. Bai, I. Ozdur, X. Zhou, and G. Li, "Supermodes for optical transmission," *Opt. Express*, vol. 19, pp. 16653–16664, 2011.
[8] R. R. Thomson, T. A. Birks, S. G. Leon-Saval, A. K. Kar, and J. Bland-Hawthorn, "Ultrafast laser inscription of an integrated photonic lantern," *Opt. Express*, vol. 19, pp. 5698–5705, 2011.
[9] D. Noordegraaf, P. M. Skovgaard, M. D. Nielsen, and J. Bland-Hawthorn, "Efficient multi-mode to single-mode coupling in a photonic lantern," *Opt. Express*, vol. 17, pp. 1988–1994, 2009.
[10] D. Noordegraaf, P. M. W. Skovgaard, M. D. Maack, J. Bland-Hawthorn, R. Haynes, and J. Lægsgaard, "Multi-mode to single-mode conversion in a 61 port photonic lantern," *Opt. Express*, vol. 18, pp. 4673–4678, 2010.
[11] S. G. Leon-Saval, N. K. Fontaine, J. R. Salazar-Gil, B. Ercan, R. Ryf, and J. Bland-Hawthorn, "Mode-selective photonic lanterns for space-division multiplexing," *Opt. Express*, vol. 22, pp. 1036–1044, 2014.
[12] G. Labroille, B. Denolle, P. Jian, P. Genevaux, N. Treps, and J.-F. Morizur, "Efficient and mode selective spatial mode multiplexer based on multi-plane light conversion," *Opt. Express*, vol. 22, pp. 15599–15607, 2014.
[13] S. Yerolatsitis, I. Gris-Sánchez, and T. A. Birks, "Adiabatically-tapered fiber mode multiplexers," *Opt. Express*, vol. 22, pp. 608–617, 2014.
[14] R. Ryf, M. A. Mestre, A. Gnauck, S. Randel, C. Schmidt, R. Essiambre, P. Winzer, R. Delbue, P. Pupalaikis, A. Sureka, Y. Sun, X. Jiang, D. Peckham, A. H. McCurdy, and R. Lingle, "Low-loss mode coupler for mode-multiplexed transmission in few-mode fiber," presented at the Optical Fiber Communication Conf. Expo./Nat. Fiber Optic Engineers Conf., Los Angeles, CA, USA, 2012, Paper PDP5B.5.
[15] H. Chen, V. A. J. M. Sleiffer, B. Snyder, M. Kuschnerov, R. G. H. Uden, Y. van Jung, C. M. Okonkwo, O. Raz, P. O'Brien, H. de Waardt, and A. M. J Koonen, "Demonstration of a photonic integrated mode coupler

with MDM and WDM transmission," *IEEE Photon. Technol. Lett.*, vol. 25, no. 21, pp. 2039–2042, Nov. 2013.
[16] G. Li, N. Bai, N. Zhao, and C. Xia, "Space-division multiplexing: the next frontier in optical communication," *Adv. Opt. Photon.*, vol. 6, pp. 413–487, 2014.
[17] K.-P. Ho and J. M. Kahn, "Mode-dependent loss and gain: Statistics and effect on mode-division multiplexing," *Opt. Express*, vol. 19, pp. 16612–16635, 2011.
[18] M. Blau and D. M. Marom, "Optimization of spatial aperture-sampled mode multiplexer for a three-mode fiber," *Photon. Technol. Lett.*, vol. 24, no. 23. pp. 2101–2104, 2012.
[19] S. Warm and K. Petermann, "Splice loss requirements in multi-mode fiber mode-division-multiplex transmission links," *Opt. Express*, vol. 21, pp. 519–532, 2013.
[20] P. J. Winzer and G. J. Foschini, "Optical MIMO-SDM system capacity," presented at the Optical Fiber Communications Conf. Exhib., San Francisco, CA, USA, 2014, Paper Th1J.1.
[21] P. Winzer, "Spatial multiplexing in fiber optics: The 10X scaling of metro/core capacities," *Bell Labs Tech. J.*, vol. 19, pp. 22–30, 2014.
[22] A. Andrusier, M. Shtaif, C. Anonelli, and A. Mecozzi, "Characterization of mode dependent loss in SDM systems," presented at the Optical Fiber Communications Conf. Exhib., San Francisco, CA, USA, 2014, Paper Th1J.2.
[23] N. K. Fontaine, R. Ryf, J. Bland-Hawthorn, and S. G. Leon-Saval, "Geometric requirements for photonic lanterns in space division multiplexing," *Opt. Express*, vol. 20, pp. 27123–27132, 2012.
[24] R. Ryf, N. K. Fontaine, and R. J. Essiambre, "Spot-based mode couplers for mode-multiplexed transmission in few-mode fiber," *IEEE Photon. Technol. Lett.*, vol. 24, no. 21, pp. 1973–1976, Nov. 2012.
[25] J. von Hoyningen-Huene, R. Ryf, and P. Winzer, "LCoS-based mode shaper for few-mode fiber," *Opt. Express*, vol. 21, pp. 18097–18110, 2013.
[26] A. M. Yao and M. J. Padgett, "Orbital angular momentum: Origins, behavior and applications," *Adv. Opt. Photon.*, vol. 3, pp. 161–204, 2011.
[27] Y. Yue, Y. Yan, N. Ahmed, J. Yang, L. Zhang, Y. Ren, H. Huang, S. Dolinar, M. Tur, and A. Willner, "Mode and propagation effects of optical orbital angular momentum (OAM) modes in a ring fiber," presented at the Optical Fiber Communication Conf., Los Angeles, CA, USA, 2012, Paper OM2D.2.
[28] Y. Yan, J. Wang, L. Zhang, J. Y. Yang, I. M. Fazal, N. Ahmed, B. Shamee, A. E. Willner, K. Birnbaum, and S. Dolinar, "Fiber coupler for generating orbital angular momentum modes," *Opt. Lett.*, vol. 36, pp. 4269–4271, 2011.
[29] Y. Yan, Y. Yue, H. Huang, J.-Y. Yang, M. R. Chitgarha, N. Ahmed, M. Tur, S. J. Dolinar, and A. E. Willner, "Efficient generation and multiplexing of optical orbital angular momentum modes in a ring fiber by using multiple coherent inputs," *Opt. Lett.*, vol. 37, pp. 3645–3647, 2012.
[30] B. Guan, R. Scott, C. Qin, N. Fontaine, T. Su, C. Ferrari, M. Cappuzzo, F. Klemens, B. Keller, M. Earnshaw, and S. Yoo, "Free-space coherent optical communication with orbital angular, momentum multiplexing/demultiplexing using a hybrid 3D photonic integrated circuit," *Opt. Express*, vol. 22, pp. 145–156, 2014.
[31] C. Doerr, N. Fontaine, M. Hirano, T. Sasaki, L. Buhl, and P. Winzer, "Silicon photonic integrated circuit for coupling to a ring-core multimode fiber for space-division multiplexing," presented at the 37th Eur. Conf. Exhib. Optical Communications, Geneva, Switzerland, 2011, Paper Th.13.A.3.
[32] N. K. Fontaine, C. R. Doerr, M. A. Mestre, R. Ryf, P. Winzer, L. Buhl, Y. Sun, X. Jiang, and R. Lingle, "Space-division multiplexing and all-optical MIMO demultiplexing using a photonic integrated circuit," presented at the Optical Fiber Communication Conf. Expo./Nat. Fiber Optic Engineers Conf., Los Angeles, CA, USA, 2012, Paper PDP5B.1.
[33] N. Bozinovic, Y. Yue, Y. Ren, M. Tur, P. Kristensen, H. Huang, A. E. Willner, and S. Ramachandran, "Terabit-scale orbital angular momentum mode division multiplexing in fibers," *Science*, vol. 340, pp. 1545–1548, 2013.
[34] A. E. Willner, "Orbital angular momentum transmission," presented at the Eur. Conf. Exhib. Optical Communication, London, U.K., 2013, Paper Mo.4.A.1.
[35] X. Tan, B-Y. Gu, G-Z. Yang, and B.-Z. Dong, "Diffractive phase elements for beam shaping: a new design method," *Appl. Opt.*, vol. 34, pp. 1314–1320, 1995.
[36] G. Zhou, X. Yuan, P. Dowd, Y-L. Lam, and Y-C. Chan, "Design of diffractive phase elements for beam shaping: hybrid approach," *J. Opt. Soc. Amer. A*, vol. 18, pp. 791–800, 2001.
[37] B. Fracasso, N. Nochez, M. Desmons, and F. Ghorbel, "An iterative approach to geometric transformations with diffractive optics," *Opt. Commun.*, vol. 133, pp. 355–364, 1997.
[38] J. L. Kreuzer, "Coherent light optical system yielding an output beam of desired intensity distribution at a desired equiphase surface," U.S. Patent 3 476 463 Nov. 4, 1969.

Authors' biographies not available at the time of publication.